Computing the Set of Epsilon-Efficient Solutions in Multiobjective Space Mission Design

Oliver Schütze*
CINVESTAV-IPN, San Pedro Zacatenco, 07360, Mexico

Massimiliano Vasile[†]
University of Strathclyde, Glasgow, G1 1XJ, United Kingdom

and

Carlos A. Coello Coello[‡]
CINVESTAV-IPN, San Pedro Zacatenco, 07360, Mexico

DOI: 10.2514/1.46478

In this work, we consider multiobjective space mission design problems. We will start from the need, from a practical point of view, to consider in addition to the (Pareto) optimal solutions also nearly optimal ones. In fact, extending the set of solutions for a given mission to those nearly optimal significantly increases the number of options for the decision maker and gives a measure of the size of the launch windows corresponding to each optimal solution, i.e., a measure of its robustness. Whereas the possible loss of such approximate solutions compared to optimal—and possibly even 'better'—ones is dispensable. For this, we will examine several typical problems in space trajectory design—a biimpulsive transfer from the Earth to the asteroid Apophis and two low-thrust multigravity assist transfers—and demonstrate the possible benefit of the novel approach. Further, we will present a multiobjective evolutionary algorithm which is designed for this purpose.

I.   Introduction

IN a variety of applications in industry and finance, a problem arises that several objective functions have to be optimized concurrently leading to *multiobjective optimization problems* (MOPs). For instance, in space mission design, which we address here, about 50% of the cost of a mission is due to the space segment, including launch, and 50% due to the ground segment, i.e., the cost of operations. The cost of the space segment, in particular of the launch, can be related to the mass of the spacecraft and to the total Δv (total variation of the linear velocity of the spacecraft) required to reach a given target. The total Δv has a direct impact on the mass of propellant onboard the spacecraft and on the required launch capabilities. In other words, the higher the Δv and the mass of the spacecraft, the higher the cost of the launch. Of course, the launch capabilities are limited, therefore for every spacecraft mass there is an upper limit on the possible Δv; in this paper, however, we are not considering that limit. The cost of operations is directly related to the total mission time, and in the case of an interplanetary transfer to the total time of flight.

---

* Associate Professor, Department of Computer Science, CINVESTAV-IPN, Av. IPN No. 2508, San Pedro Zacatenco, 07360, Mexico. schuetz@cs.cinvestav.mx.
† Reader, SpaceART, Department of Mechanical Engineering, AIAA Member.
‡ Professor, Department of Computer Science, CINVESTAV-IPN, Av. IPN No. 2508, San Pedro Zacatenco, 07360, Mexico.

Therefore, for the optimal design of a generic interplanetary trajectory, we can identify two objective functions: time of flight and total Δv (or total propellant consumption) [1–4].

The quality of a solution in an MOP is generally defined by its Pareto optimality, i.e., a solution is Pareto optimal if no other solution is better over all the objective values. The set of Pareto optimal solutions forms a Pareto set in the parameter space and a Pareto front in the objective space. As shown later in this paper and also by Vasile [5], the Pareto set can cover only a small portion of the parameter space, corresponding to a limited number of launch dates. During the design of a space mission, in particular in the early phase, it would be desirable, instead, to have also the solutions in the neighborhood of the optimal ones. A knowledge of the neighboring solutions will help in the identification of the extension of the launch window associated to each optimal solution, i.e., the range of possible launch dates for which both the total Δv and the time of flight are below a given threshold. In other words, a knowledge of the neighboring solutions gives a measure of the robustness of an optimal solution. Note that designing for the suboptimal points increases the reliability of the mission since it gives the freedom to deviate from the chosen design point with little or no penalty. This holds true also for Pareto optimal solutions. It is therefore desirable to have a whole range of nearly Pareto optimal solutions for each Pareto point. Furthermore, it would be desirable to extend as much as possible the number of launch opportunities.

As a motivating example, we consider the MOP in Sec. IV.C, which corresponds to the design of a low-thrust multigravity assist trajectory from the Earth to Mercury following the sequence Earth–Venus–Mercury (EVMe). Let us consider the two points x_i with images $F(x_i)$, $i = 1, 2$:

$$x_1 = (782, 1288, 1788), \quad F(x_1) = (0.462, 1001.7)$$

$$x_2 = (1222, 1642, 2224), \quad F(x_2) = (0.463, 1005.3)$$

The two objectives are the propellant mass fraction—i.e., the portion of the vehicle's mass which does not reach the destination—and the time of flight (in days). In the domain, the first parameter is of particular interest: it determines the departure time from the Earth (in days after 01.01.2000), i.e., the launch time of the mission. The image $F(x_1)$ is less than $F(x_2)$ in both components, and thus, x_1 can be considered to be "better" than x_2 (x_1 is said to *dominate* x_2). However, the difference in image space is small: the mass fraction of the two solutions differs by 0.001 which makes 0.1% of the total mass, and the flight time differs by 4 days for a transfer which takes almost 3 years. In case the decision maker (DM) is willing to accept this deterioration, it will offer him/her a second choice in addition to x_1 for the realization of the transfer: although the two solutions offer "similar" characteristics in image space, this is not the case in the design space, since the starting times for the two transfers differ by 440 days. The two solution, therefore, represent two distinct launch opportunities.

In this case, the identification of two solutions increases the reliability of the design, because one solution can become the baseline and the other can serve as backup, with almost identical cost. This paper will show the benefits of considering, in addition to the Pareto optimal trajectories, also the set of approximate (or nearly optimal) solutions. Furthermore, it will present one way to compute this enlarged set of interest with a reasonable computational effort through a novel evolutionary algorithm based on a particular archiving technique.

The field of evolutionary multiobjective optimization is well-studied and multiobjective evolutionary algorithms (MOEAs) have been successfully applied in a number of domains, most notably engineering applications [6]. Approximate solutions in multiobjective optimization have been studied by many researchers so far [7–9], however, the only studies which deal (albeit theoretically) with the computation of the entire set of approximate solutions have been undertaken by Schütze et al. [2,10]. A first attempt to investigate the benefit of considering approximate solutions in space mission design has been done by Vasile and Locatelli [11], albeit for the single-objective case.

The additional consideration of approximate solutions in multiobjective space mission design problems is new and will be addressed in this paper (a preliminary study of this paper can be found in Schütze et al. [12]). Crucial for this approach is the efficient computation of the enlarged set of "optimal" points (the second scope of this paper) since in many cases the "classical" multiobjective approach is a challenge itself. For this, we will propose an algorithm which is modeled on the basis of the ϵ-MOEA [13] and which is adapted to the current context. Note that "classical" archiving/selection strategies—e.g., the ones reported by Hanne [14], Rudolph and Agapie [15], Laumanns et al. [7] and Knowles and Corne [16] or the ones most state-of-the-art MOEAs such as NSGA-II [17] use—store sets of mutually non-dominating points (which means that, e.g., the points x_1 and x_2 in the above example will never be

stored *jointly*). That is, these selection mechanisms—though they accomplish an excellent job in approximating the efficient set—cannot be adopted for our purposes.

The remainder of this paper is organized as follows. In Sec. II, we give the required background which includes the statement of the space mission design problem under consideration. In Sec. III, we propose a new genetic algorithm for the computation of the set of approximate solutions and present further on in Sec. IV some numerical results. Finally, we conclude in Sec. V.

II.   Background

Here we will shortly recall the required background for the sequel: the concept of multiobjective optimization including our definition of nearly optimality and the design problems under consideration.

A. Multiobjective Optimization

In the following, we consider continuous multiobjective optimization problems

$$\min_{x \in Q}\{F(x)\} \qquad \text{(MOP)}$$

where the domain $Q \subset \mathbb{R}^n$ is compact and $F : Q \to \mathbb{R}^k$ is defined as the vector of the objective functions

$$F(x) = (f_1(x), \dots, f_k(x)) \qquad (1)$$

and where each objective $f_i : Q \to \mathbb{R}$ is continuous. The concept of optimality we use here was first introduced by Pareto [18].

Definition 1: Let $v, w \in Q$. Then the vector v is less than w ($v <_p w$), if $v_i < w_i$ for all $i \in \{1, \dots, k\}$. The relation $\leqslant_p$ is defined analogously. $y \in Q$ is *dominated* by a point $x \in Q$ ($x \prec y$) with respect to (MOP) if $F(x) \leqslant_p F(y)$ and $F(x) \neq F(y)$. $x \in Q$ is called a *Pareto optimal point* or *Pareto point* if there is no $y \in Q$ which dominates x.

The set of all Pareto optimal solutions is called the *Pareto set* (denoted by P_Q). The image of the Pareto set $F(P_Q)$ is called the *Pareto front*. We now define another notion of dominance which we use to define approximate solutions.

Definition 2: Let $\epsilon = (\epsilon_1, \dots, \epsilon_k) \in \mathbb{R}_+^k$ and $x, y \in Q$.
   a)   Vector x is said to ϵ-dominate y ($x \prec_\epsilon y$) with respect to (MOP) if $F(x) - \epsilon \leqslant_p F(y)$ and $F(x) - \epsilon \neq F(y)$.
   b)   Vector x is said to $-\epsilon$-dominate y ($x \prec_{-\epsilon} y$) with respect to (MOP) if $F(x) + \epsilon \leqslant_p F(y)$ and $F(x) + \epsilon \neq F(y)$.

The notion of $-\epsilon$-dominance [10] is, of course, analogous to the "classical" ϵ-dominance relation [8] but with a value $\tilde{\epsilon} \in \mathbb{R}_-^k$. However, we highlight it here since we use it to define our set of interest.

Definition 3: Denote by $P_{Q,\epsilon}$ the set of points in $Q \subset \mathbb{R}^n$ which are not $-\epsilon$-dominated by any other point in Q, i.e.,

$$P_{Q,\epsilon} := \{x \in Q \mid \nexists y \in Q : y \prec_{-\epsilon} x\} \qquad (2)$$

The set $P_{Q,\epsilon}$ contains all ϵ-efficient solutions, i.e., solutions which are optimal up to a given (small) value of ϵ. Figure 1 gives two examples.

Algorithm 1 gives a framework of a generic stochastic multiobjective optimization algorithm, as the one we consider in this work. Here, $Q \subset \mathbb{R}^n$ denotes the domain of the MOP, P_j the candidate set (or population) of the generation process at iteration step j, and A_j the corresponding archive.
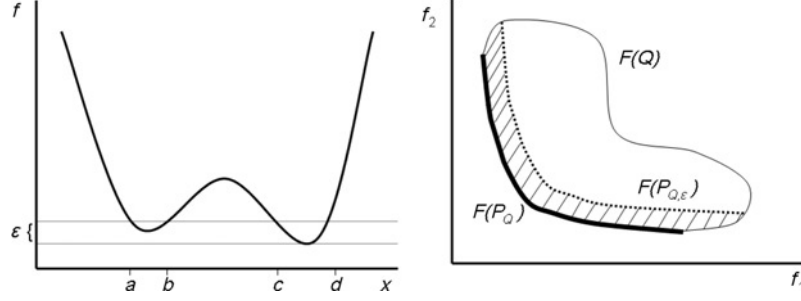
Fig. 1 Two different examples for sets $P_{Q,\epsilon}$. At the left, we show the case for $k = 1$ and in parameter space with $P_{Q,\epsilon} = [a, b] \cup [c, d]$. Note that the image solutions $f([a, b])$ are nearly optimal (measured in objective space), but that the entire interval $[a, b]$ is not "near" to the optimal solution which is located within $[c, d]$. At the right, we show an example for $k = 2$ in image space, $F(P_{Q,\epsilon})$ is the approximate Pareto front.

Algorithm 1 Generic stochastic search algorithm

1: $P_0 \subset Q$ drawn at random
2: $A_0 = \text{ArchiveUpdate}(P_0, \emptyset)$
3: **for** $j = 0, 1, 2, \ldots$ **do**
4:     $P_{j+1} = \text{Generate}(P_j)$
5:     $A_{j+1} = \text{ArchiveUpdate}(P_{j+1}, A_j)$
6: **end for**

To measure the approximation quality of the outcome set of an MOEA, we will use the semi-distance dist and the *Hausdorff distance d_H*:

Definition 4: Let $u, v \in \mathbb{R}^n$ and $A, B \subset \mathbb{R}^n$. The maximum norm distance d_∞, dist$(\cdot, \cdot)$, and $d_H(\cdot, \cdot)$ are defined as follows:

    a) $d_\infty(u, v) := \max_{i=1,\ldots,n} |u_i - v_i|$;
    b) $\text{dist}(u, A) := \inf_{v \in A} d_\infty(u, v)$;
    c) $\text{dist}(B, A) := \sup_{u \in B} \text{dist}(u, A)$;
    d) $d_H(A, B) := \max\{\text{dist}(A, B), \text{dist}(B, A)\}$.

Note that dist is not symmetric. For instance, for $A = [0, 1]$ and $B = [0, 2]$ it is dist$(A, B) = 0$ (since $A \subset B$) and dist$(B, A) = 1$.

Schütze et al. [2] showed that, under certain (mild) conditions on the set $P_{Q,\epsilon}$ of the MOP and under the assumption

$$\forall x \in Q \text{ and } \forall \delta > 0 : \quad P(\exists l \in \mathbb{N} : P_l \cap B_\delta(x) \cap Q \neq \emptyset) = 1 \tag{3}$$

on Generate( ), the Algorithm 1 equipped with Algorithm 2 as archiver generates a sequence of archives A_i which converges with probability one toward an approximation of the set of interest (hereby, $P(A)$ denotes the probability for event A). More precisely, there exists with probability one an $l_0 \in \mathbb{N}$ such that, for all $l \geqslant l_0$,

$$d_H(F(P_{Q,\epsilon}), F(A_l)) \leqslant \max(\Delta, \text{dist}(F(P_{Q,\epsilon+2\Delta}), F(P_{Q,\epsilon}))) \tag{4}$$

where $\Delta < \min_{i=1,\ldots,k} \epsilon_i$ and Δ^* are parameters used to determine the granularity of the approximation: the archive ensures (line 3 of Algorithm 2) that the minimal difference between two archive images is bounded, i.e.,

$$\|F(a_1) - F(a_2)\|_\infty \geqslant \Delta^* \quad \forall a_1, a_2 \in A_l : a_1 \neq a_2, \forall l \in \mathbb{N} \tag{5}$$

resulting in a natural 'spread' of the archive entries by which it follows that no additional spreading mechanisms such as niching techniques [19,20] are required in a MOEA which is equipped with this archiver; $\Delta^* < \Delta$ is required for theoretical purposes, in practice $\Delta^* = \Delta$ can be chosen, for a thorough discussion we refer to Schütze et al. [2].

Algorithm 2 $A := $ ArchiveUpdate $P_{Q,\epsilon}$ (P, A_0, Δ)

Require: population P, archive A_0, $\Delta \in \mathbb{R}_+$, $\Delta^* \in (0, \Delta)$
Ensure: updated archive A
 1: $A := A_0$
 2: **for all** $p \in P$ **do**
 3:    **if** $\nexists a_1 \in A : a_2 \prec_{-\epsilon} p$ and $\nexists a_2 \in A : d_\infty(F(a_2), F(p)) \leqslant \Delta^*$ **then**
 4:       $A := A \cup \{p\}$
 5:       **for all** $a \in A$ **do**
 6:          **if** $p \prec_{-(\epsilon+1\Delta)} a$ **then**
 7:             $A := A \backslash \{a\}$
 8:          **end if**
 9:       **end for**
10:    **end if**
11: **end for**

B. The Design Problems

In the following we will analyze a few examples taken from two classes of typical problems in space trajectory design: a biimpulsive transfer from the Earth to the asteroid Apophis, and two low-thrust multigravity assist transfers from the Earth to a planet.

BIIMPULSE PROBLEM. For the biimpulsive case, the propellant consumption is a function of the velocity change, or Δv [21], required to depart from the Earth and to rendezvous with a given celestial body. Both the Earth and the target celestial body are point masses with the only source of gravity attraction being the Sun. Therefore, the spacecraft is assumed to be initially at the Earth, flying along its orbit. The first velocity change, or Δv_1, is used to leave the orbit of the Earth and put the spacecraft into a transfer orbit to the target. The second change in velocity, or Δv_2, is then used to inject the spacecraft into the target's orbit.

The two Δv's are a function of the positions of the Earth and the target celestial body at the time of departure t_0 and at the time of arrival $t_f = t_0 + T$, where T is the time of flight. Thus, the MOP under consideration reads as follows:

$$\text{minimize:} \quad \begin{cases} \Delta v_1 + \Delta v_2 \\ T \end{cases} \tag{6}$$

MLTGA PROBLEM. It is here proposed to use a particular model for multigravity assist low-thrust trajectories (MLTGA). Low-thrust arcs are modeled through a shaping approach based on the exponential sinusoid proposed by Petropoulos Longuski et al. [22]. The spacecraft is assumed to be moving in a plane subject to the gravity attraction of the Sun and to the control acceleration $\mathbf{F} = [F \cos \alpha, F \sin \alpha]^T$ of a low-thrust propulsion engine. The dynamic equations governing the motion of the spacecraft can be written in polar coordinates as follows:

$$\ddot{r} - r\dot{\theta}^2 + \frac{\mu}{r^2} = F \sin \alpha$$

$$\frac{1}{r}\frac{d}{dt}(r^2\dot{\theta}) = F \cos \alpha$$

where α is the thrust steering angle measured clockwise from the axis perpendicular to r in the direction of motion. For this particular dynamics, Petropoulos proposed to use the following shaping function for the radius as a function of the polar angle θ:

$$r = k_0 e^{k_1 \sin(k_2\theta + \phi)}$$

Then, if the thrust vector is aligned with the velocity vector, the flight path angle γ and the thrust steering angle α are equal. If $\gamma = \alpha$, then the thrust history and the polar angle history are uniquely determined and the control

acceleration is given by

$$F = \frac{\mu}{r^2} \frac{\tan \gamma}{2 \cos \gamma} \left[\frac{1}{\tan^2 \gamma + k_1 k_2^2 s + 1} - \frac{k_2^2(1 - 2k_1 s)}{(\tan^2 \gamma + k_1 k_2^2 s + 1)^2} \right] \tag{7}$$

with the time variation of the true anomaly given by

$$\dot{\theta}^2 = \left(\frac{\mu}{r^3} \right) \frac{1}{\tan^2 \gamma + k_1 k_2^2 s + 1} \tag{8}$$

and the flight path angle given by

$$\tan \gamma = k_1 k_2 \cos(k_2 \theta + \phi) \tag{9}$$

with $s = \sin(k_2 \theta + \phi)$. Now, by solving the following integral:

$$\Delta t = \int \frac{d\theta}{\sqrt{(\mu/r^3)(1/(\tan^2 \gamma + k_1 k_2^2 s + 1))}} \tag{10}$$

one can compute the actual time of flight.

The exponential sinusoid expresses the variation of the radius as a function of the polar angle θ and depends on three shaping parameters k_0, k_1, k_2 plus a phase parameter ϕ. By fixing the initial and final radius for $\theta = 0$ and $\theta = \bar{\theta}$, respectively,

$$r_1 = k_0 e^{k_1 \sin(\phi)}$$
$$r_2 = k_0 e^{k_1 \sin(k_2 \bar{\theta} + \phi)} \tag{11}$$

two of the three parameters can be computed as a function of the others.

The two position radii and the angular difference $\bar{\theta}$ between the departure and the arrival points can be computed from the ephemerides of the departure and arrival planets or other celestial bodies (in this work we used analytical ephemerides). In this case it is normally required that the transfer trajectory going from one planet to the other is flown in a given time T. This implies that the actual time of flight must be equal to the required time of flight in order to have a physical solution:

$$\Delta t - T = 0 \tag{12}$$

If now this time constraint is solved, a third parameter can be determined and the exponential sinusoid becomes a single-valued function (for more details on the solution of (12) please refer to Izzo [23]).

In this form, given the transfer time and the two position vectors at the beginning and at the end of the transfer we can compute the velocities at the two extremal points and the thrust profile. Since only one shaping parameter is free, it is not possible to optimize the value of the velocities at the boundaries plus the thrust profile but the problem is equivalent to the Lambert's problem for conic arcs.

Furthermore, some analysis [22] reveals that the exponential sinusoid gives physical solutions whenever $k_1 k_2^2 < 1$. This limit will be used in the remainder of this paper to limit the values of the shaping parameter k_2.

Gravity assist maneuvers are modeled with a linked-conic approximation: the maneuvers is instantaneous (i.e., no variation in the position of the spacecraft) and produces a deflection of the planetocentric velocity vector, the planet is reduced to a point mass with no gravity, the deflection angle β_{swing} is a function of the mass of the planet and of the incoming velocity, such that

$$\tilde{\mathbf{v}}_{\text{in}}^T \tilde{\mathbf{v}}_{\text{out}} = -\tilde{v}_i^2 \cos \beta_{\text{swing}} \tag{13}$$

and

$$\beta_{\text{swing}} = 2 \arccos \left(\frac{\mu_p}{\tilde{v}_{\text{in}}^2 r_p + \mu_p} \right) \tag{14}$$

where μ_p is the gravity constant of the swing-by planet, $\tilde{\mathbf{v}}_{\text{in}}$ and $\tilde{\mathbf{v}}_{\text{out}}$ are the planetocentric incoming and outgoing velocity vectors and r_p is the radius of the pericenter of the swing-by hyperbola.

Since the value of the velocities at the boundaries is not completely free, to give an incoming velocity vector is not possible, in general, to match every possible outgoing velocity vector.

A match can be obtained by inserting a ΔV correction at the pericenter of the hyperbola of the swing-by. This model will be called powered swing-by model or powered swing-by in the following.

Here we describe the biobjective optimization problem that we consider in the sequel. The two objectives are the propellant mass fraction and the flight time which result by a given trajectory.

For $N + 1$ celestial bodies, a sequence of thrust legs is then assembled to all the others through a sequence of powered swing-bys. Each thrust leg is modeled through a shape-based method based on exponential sinusoids [22] and the first objective is given as

$$\begin{aligned} \text{minimize:} \quad & J(y) \\ \text{subject to:} \quad & r_p \geqslant r_{\min} \end{aligned} \tag{15}$$

The complete solution vector is then defined as follows:

$$y = [t_0, T_1, k_{2,1}, n_1, \ldots, T_i, k_{2,i}, n_i, \ldots, T_N, k_{2,N}, n_N]^T \tag{16}$$

where $k_{2,i}$ is the ith shaping parameter for the exponential sinusoid and n_i the number of revolutions around the Sun. The objective function J is then defined as follows:

$$J = 1 - e^{-((\Delta V_{\mathrm{GA}} + \Delta V_0)/(g_0 I_{\mathrm{sp1}})) + (\Delta V_{\mathrm{LT}}/(g_0 I_{\mathrm{sp2}}))} \tag{17}$$

where ΔV_{GA} is the sum of all the ΔV's (variation in velocity) required to correct every gravity assist maneuver, ΔV_0 is the departure maneuver, and ΔV_{LT} is the sum of the total ΔV of each low-thrust leg. The two specific impulses I_{sp1} and I_{sp2} are, respectively, for a chemical engine and for a low-thrust engine and g_0 is the gravity acceleration on the surface of the Earth.

For the tests in this paper, we used $I_{\mathrm{sp1}} = 315\,\mathrm{s}$ and $I_{\mathrm{sp2}} = 2500\,\mathrm{s}$. Note that, the computation of a transfer arc with the exponential sinusoid does not require the time history of the mass of the spacecraft. The time history of the mass would be required to compute the actual thrust profile along the transfer arc. The integration of (7), instead, gives directly the Δv due to the low-thrust propulsion.

The objective function (17) is particularly appealing because it has values ranging from 0, best transfer, to 1, worst transfer. In addition, the impulsive Δv and the low-thrust Δv are weighted in such a way that the use of low-thrust is favored with respect to the use of the impulsive corrections. Note that the scope of this paper is not to demonstrate the suitability of the exponential sinusoid model for the design of MLTGA trajectories but rather to demonstrate the benefit of the additional use of approximate solutions. The overall process for the composition of a MLTGA trajectory with the exponential sinusoid model can be summarized with the following steps (see Fig. 2):

- For each departure date t_0 and N legs with transfer times $\mathbf{T} = [T_1, \ldots, T_i, \ldots, T_N]^T$.
- Compute a low-thrust arc through the exponential sinusoid model from planet i to planet $i + 1$ (see the transfer from A to B as an example in Fig. 2).
- Compute the incoming heliocentric velocity vector $\mathbf{v}_{\mathrm{in}}$ and the corresponding planetocentric velocity vector $\tilde{\mathbf{v}}_{\mathrm{in}}$.
- Compute a low-thrust arc through the exponential sinusoid model from planet $i + 1$ to planet $i + 2$ (see the transfer from B to C as an example in Fig. 2).
- Compute the required heliocentric outgoing velocity vector $\mathbf{v}_{\mathrm{rout}}$ and the corresponding required planetocentric velocity vector $\tilde{\mathbf{v}}_{\mathrm{rout}}$.
- Compute the achievable planetocentric outgoing velocity vector $\tilde{\mathbf{v}}_{\mathrm{aout}}$ with pericenter radius $r_p \geqslant r_{\min}$.
- If $\tilde{\mathbf{v}}_{\mathrm{aout}} \neq \tilde{\mathbf{v}}_{\mathrm{rout}}$, then compute the matching ΔV_i at the pericenter of the hyperbola.
- Compute the launch impulsive maneuver ΔV_0.
- Compute the arrival impulsive maneuver ΔV_N.
- Compute the low-thrust ΔV_{LT}.
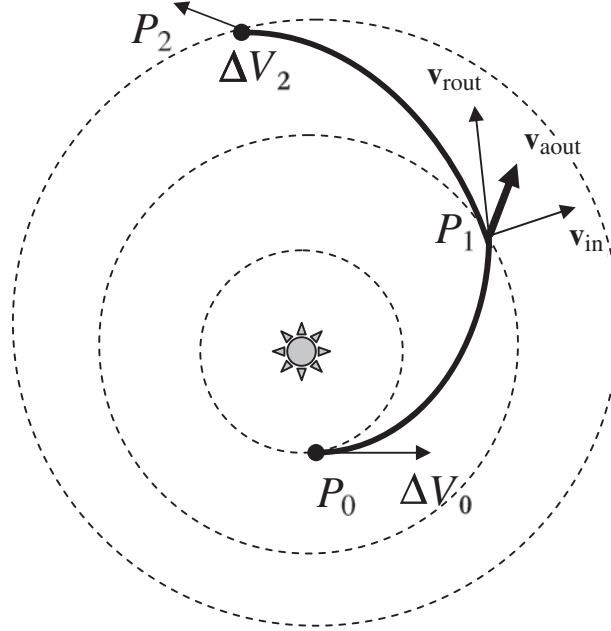- Compute the sum of all ΔV's.

Fig. 2 Composition of a whole MLTGA trajectory for the exponential sinusoid model.

The arrival at planet i corresponds to a time $t_i = t_{i-1} + T_i$, therefore the final time at the end of the transfer is t_N, while the corrective ΔV's are computed for all the indexes from 2 to $N - 1$.

Note that, although all the low-thrust arcs modeled with the exponential sinusoid are planar trajectories, the whole trajectory develops in the three-dimensional space. Therefore, the ΔV required for every plane change is obtained through an impulsive maneuver at the boundaries of the low-thrust arc and included in ΔV_0, ΔV_N, or in the ΔV_{GA}.

The second objective of the MOP which we address in this work is simply given by the *flight time $t_N - t_0$* used for the selected trajectory. This objective is of great importance for the design process since the transfer can take several years.

Thus, the MOP under consideration reads as follows:

$$\text{minimize:} \quad \begin{cases} J(y) \\ t_N - t_0 \end{cases} \tag{18}$$

$$\text{subject to:} \quad r_p \geqslant r_{\min}$$

III.   A MOEA for the Computation of $P_{Q,\epsilon}$

Here, we present a novel evolutionary algorithm, $P_{Q,\epsilon}$-MOEA, for the computation of the set of approximate solutions, and present further on some performance indicators which aim to measure the approximation quality of a given outcome set.

A. The Algorithm

The evolutionary strategy, $P_{Q,\epsilon}$-MOEA, we propose here is a steady-state archive-based MOEA. In the beginning, the archiver is fed with randomly chosen elements from Q, where ArchiveUpdate $P_{Q,\epsilon}$ is taken as archiver. In the ith step of the algorithm two parent solutions p_1 and p_2 are chosen at random from the current archive A_i from which the two offspring o_1 and o_2 are generated as follows: either crossover is performed (with a given probability p_c) or mutation is performed on both archive entries. The offspring is finally used to update A_i leading to the new archive A_{i+1} (see Algorithm 3 and Fig. 3). For the numerical results that we will present in the sequel, we have used the simulated binary crossover and the polynomial mutation, respectively [24].

Algorithm 3 $P_{Q,\epsilon}$-MOEA

1: $P_0 \subset Q$ drawn at random
2: $A_0 := \text{ArchiveUpdate} P_{Q,\epsilon}(P_0, \emptyset)$
3: **for** $l = 0, 1, 2, \ldots$ **do**
4:     choose $p_1, p_2 \in A_l$ at random
5:     perform generational operators on p_1, p_2 leading to o_1, o_2
6:     $A_{l+1} := \text{ArchiveUpdate} P_{Q,\epsilon}(\{o_1, o_2\}, A_l)$
7: **end for**
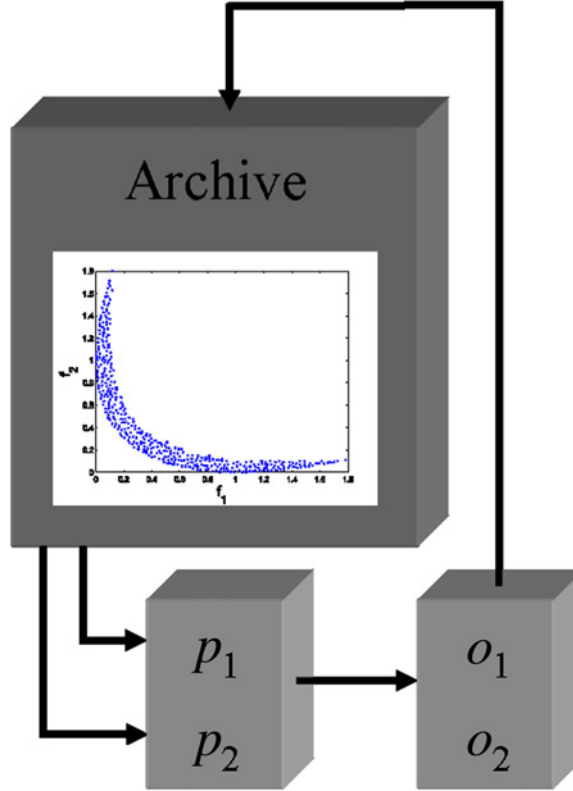
Fig. 3 Working principle of $P_{Q,\epsilon}$-MOEA.

Since the probability for mutation is positive in each step and the support of the density function of the polynomial mutation is positive on Q for each point $x \in Q$, the general assumption on the generator (3) is fulfilled. Hence, $P_{Q,\epsilon}$-MOEA generates with probability one a sequence of archives A_i which converges toward an approximation of the set of interest (compare to the Sec. II or to Schütze et al. [2]).

The $P_{Q,\epsilon}$-MOEA has been modeled on the basis of ϵ-MOEA which has been proposed by Deb et al. [13]; note that

> ..., it is observed that the steady-state MOEA is a good compromise in terms of convergence near to the Pareto-optimal front, diversity of solutions, and computational time.

There are two main differences between the two algorithms which are due to their different scopes: (i) the choice of the archivers (ϵ-MOEA heads for an approximation of the Pareto front, and is hence equipped with a different archiver) and (ii) $P_{Q,\epsilon}$-MOEA does not use a population in addition to the archive. The latter is included in ϵ-MOEA to prevent that the candidate set "collapses" when inserting strongly dominating solutions (i.e., when an entire range of archive entries is dominated by an offspring o these are discarded from the archive—when using an elitism strategy

and when heading for the Pareto front—which could result in a bad performance of the population-based approach due to the lack of candidate solutions in a certain region). We have observed that such a mechanism (and the related additional computational complexity) is not required when heading for $P_{Q,\epsilon}$. In fact, since in ArchiveUpdate $P_{Q,\epsilon}$ elements are discarded if they are $-(\epsilon + \Delta)$-dominated by an offspring o, the archiver is much more robust to such collapses.

So far, the only existing algorithm for the computation of $P_{Q,\epsilon}$ is $P_{Q,\epsilon}$-NSGA-II proposed by Schütze et al. [12], which is based on the well-known NSGA-II [17]. $P_{Q,\epsilon}$-NSGA-II uses the same ranking strategy as its base MOEA, and thus, the highest pressure of the population is taken toward the Pareto set. We have observed, however, that this could lead to problems when $P_{Q,\epsilon}$ contains connected components where the intersection with the Pareto set is empty (i.e., for each point x in such a component C, there exists an element $y \notin C$ such that $y \prec x$) since in that case such components can be overseen by the search strategy (see, for instance, the example in Sec. IV.A). Instead, the search should be performed bias-free on the entire set of approximate solutions, which was the motivation for developing the new $P_{Q,\epsilon}$-MOEA.

B. Performance Metrics

To assess the performance of an (evolutionary) algorithm, it is desirable to have a performance metric that measures the approximation quality of the outcome set. Since so far no such metric exists, we adapt here some established indicators for the classical multiobjective case to the current context. Whereas all (established) performance indicators for the treatment of classical MOPs are defined in objective space, we have to consider here in addition the approximation quality in parameter space since this is one important aspect when considering approximate solutions (see for instance the left example in Fig. 1).

Assume that we are given the set $P_{Q,\epsilon}$ analytically (or we are given a good approximation of it), then the approximation quality of a given (finite) archive $A = \{a_1, \ldots, a_l\}$ can, for example, be measured by the Hausdorff distance:

$$d_H(A, P_{Q,\epsilon}) = \max(\mathrm{dist}(A, P_{Q,\epsilon}), \mathrm{dist}(P_{Q,\epsilon}, A)) \tag{19}$$

where

$$\mathrm{dist}(A, P_{Q,\epsilon}) = \max_{i=1,\ldots,l} \min_{p \in P_{Q,\epsilon}} \|a_i - p\| \tag{20}$$

$$\mathrm{dist}(P_{Q,\epsilon}, A) = \max_{p \in P_Q} \min_{i=1,\ldots,l} \|a_i - p\| \tag{21}$$

If the value in (19) is 0, then it means that A is dense in $P_{Q,\epsilon}$ (i.e., the closure of A is equal to $P_{Q,\epsilon}$), and thus, A can be regarded as a perfect approximation. By this, it follows that small values of d_H in (19) indicate good approximations A. In case the value of d_H is not small, however, a more detailed consideration is required. One can, for instance, consider instead of (19) the two values of (20) and (21) separately: (20) measures the convergence of A toward $P_{Q,\epsilon}$ whereas (21) gives an idea about the spread of the entries of A along the set of interest. One potential drawback of the indicators (20) and (21)—and hence also of (19)—is that single outliers can give a false impression on the approximation quality, a problem which is hard to overcome when using stochastic search algorithms. Instead, the distances can be averaged leading to the following alternatives to (20) and (21), respectively,

$$\mathrm{GD}_x(A) := \frac{1}{l} \sqrt{\sum_{i=1}^{l} (\mathrm{dist}(a_i, P_{Q,\epsilon}))^2} \tag{22}$$

$$\mathrm{IGD}_x(A) := \frac{1}{m} \sqrt{\sum_{i=1}^{m} (\mathrm{dist}(p_i, A))^2} \tag{23}$$

where we assume that we are given an approximation of $P_{Q,\epsilon}$ consisting of m elements. These indicators are modifications of the generational distance [25] and the inverted generational distance [6] which are commonly used to assess the performance of MOEAs.

The above discussion is analog for a performance measure in objective space. The Hausdorff distance of the image of A toward the approximate Pareto front $F(P_{Q,\epsilon})$ is given by

$$d_H(F(A), F(P_{Q,\epsilon})) = \max(\text{dist}(F(A), F(P_{Q,\epsilon})), \text{dist}(F(P_{Q,\epsilon}), F(A))) \tag{24}$$

where

$$\text{dist}(F(A), F(P_{Q,\epsilon})) = \max_{i=1,\dots,l} \min_{p \in P_{Q,\epsilon}} \|F(a_i) - F(p)\| \tag{25}$$

$$\text{dist}(F(P_{Q,\epsilon}), F(A)) = \max_{p \in P_Q} \min_{i=1,\dots,l} \|F(a_i) - F(p)\| \tag{26}$$

The averaged distances are as follows:

$$\text{GD}_y(F(A)) := \frac{1}{l}\sqrt{\sum_{i=1}^{l}(\text{dist}(F(a_i), F(P_{Q,\epsilon})))^2} \tag{27}$$

$$\text{IGD}_y(F(A)) := \frac{1}{m}\sqrt{\sum_{i=1}^{m}(\text{dist}(F(p_i), F(A))^2} \tag{28}$$

Things change when no approximation of $P_{Q,\epsilon}$ of the MOP is at hand since in that case no statements on the approximation quality in parameter space can be made (note that $P_{Q,\epsilon}$ is based on the concept of $-\epsilon$-dominance which is defined in objective space), and we have to leave this issue for future research. For a comparison of two given outcome sets A and B in image space, we found the following indicator useful

$$\mathcal{C}_{-\epsilon}(A, B) := \frac{|\{b \in B \,:\, \exists a \in A : a \prec_{-\epsilon} b\}|}{|B|} \tag{29}$$

which is a straightforward extension of the *set coverage metric* suggested by Zitzler and Thiele [26]. Analog to the original metric, $\mathcal{C}_{-\epsilon}(A, B)$ is an unsymmetric operator which aims to get an idea of the relative spread of the two solution sets.

IV.   Numerical Results

Here we present some numerical results coming from one academic problem and three different space mission design scenarios.

A. An Academic Example

First, we consider an academic MOP in order to demonstrate the strength of the novel approach. The model is a modification of the one proposed by Rudolph et al. [27]:

$$F : \mathbb{R}^2 \to \mathbb{R}^2$$

$$F(x_1, x_2) = \begin{pmatrix} (x_1 - t_1(c + 2a) + a)^2 + (x_2 - t_2 b)^2 + \delta_t \\ (x_1 - t_1(c + 2a) - a)^2 + (x_2 - t_2 b)^2 + \delta_t \end{pmatrix} \tag{30}$$

where

$$t_1 = \text{sgn}(x_1) \min\left(\left\lceil \frac{|x_1| - a - c/2}{2a + c} \right\rceil, 1\right), \quad t_2 = \text{sgn}(x_2) \min\left(\left\lceil \frac{|x_2| - b/2}{b} \right\rceil, 1\right),$$

and

$$\delta_t = \begin{cases} 0 & \text{for } t_1 = 0 \text{ and } t_2 = 0 \\ 0.1 & \text{else} \end{cases}$$

Using $a = 0.5, b = 5, c = 5$, MOP (30) contains one global Pareto set

$$P_{0,0} = [-0.5, 0.5] \times \{0\} \tag{31}$$

as well as the following eight local Pareto sets

$$P_{-1,-1} = [-6.5, -5.5] \times \{-5\}$$
$$P_{0,-1} = [-0.5, 0.5] \times \{-5\}$$
$$P_{1,-1} = [5.5, 6.5] \times \{-5\}$$
$$P_{-1,0} = [-6.5, -5.5] \times \{0\}$$
$$P_{1,0} = [5.5, 6.5] \times \{0\}$$
$$P_{-1,1} = [-6.5, -5.5] \times \{5\}$$
$$P_{0,1} = [-0.5, 0.5] \times \{5\}$$
$$P_{1,1} = [5.5, 6.5] \times \{5\}.$$

(32)
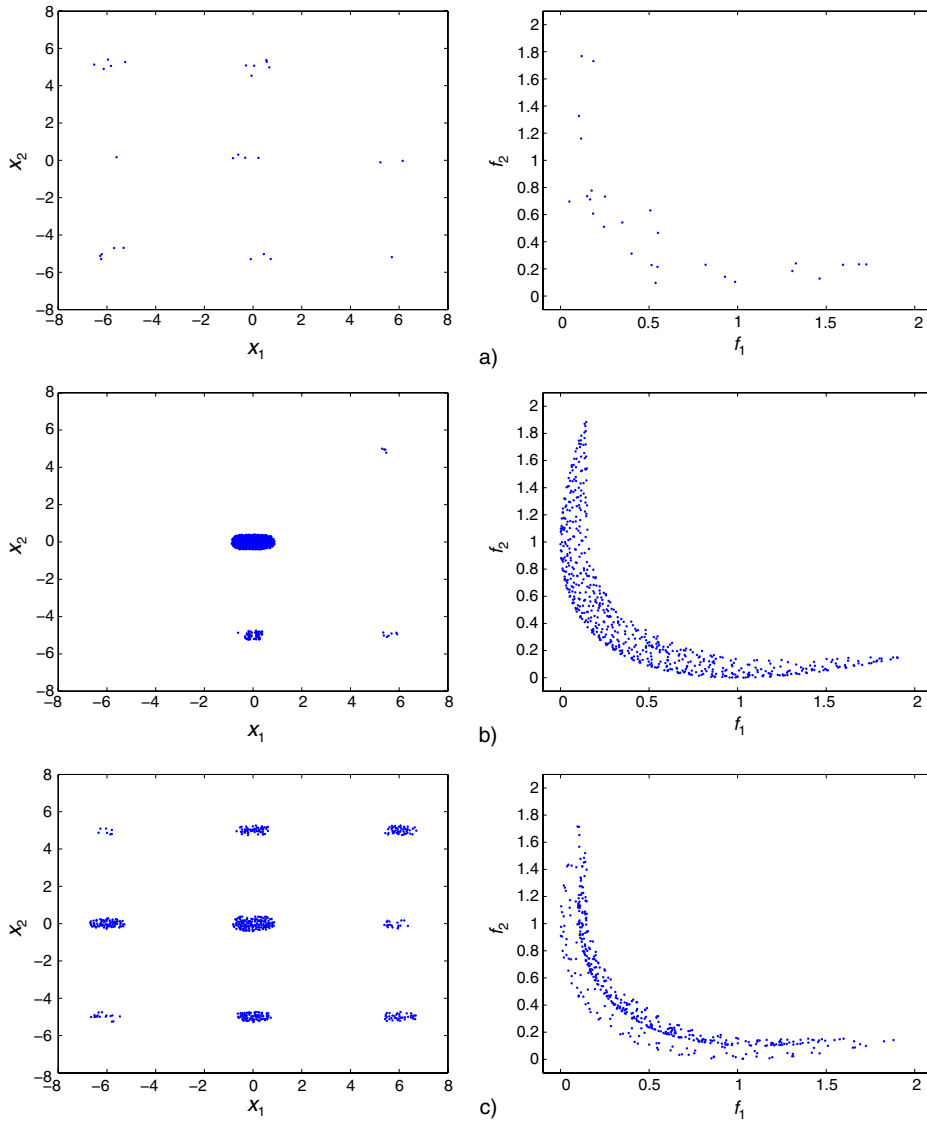
Fig. 4 Numerical results for MOP (30) for a) random search, b) $P_{Q,\epsilon}$-NSGA-II, and c) $P_{Q,\epsilon}$-MOEA, in parameter space (left) and image space (right).

Note that if δ_t would be constantly 0, the Pareto set would contain nine connected components with equal images. By the choice of δ_t, the eight images of (32) are 'lifted', and thus, when choosing, e.g., $\epsilon = (0.15, 0.15)$ only nearly optimal. In that case $P_{Q,\epsilon}$ consists of nine connected components given by neighborhoods of (31) and (32).

Figure 4 shows some numerical results of MOP (30) where we have chosen $\epsilon = (0.15, 0.15)$, $\Delta = 0.01$, and $Q = [-20, 20]^2$, i.e., $P_{Q,\epsilon}$ consists of a superset of these nine local sets. The figure shows a comparison of a random search algorithm (i.e., a random search generator has been chosen for Generate( ) in Algorithm 1), $P_{Q,\epsilon}$-NSGA-II, and $P_{Q,\epsilon}$-MOEA (using an initial population of 200 elements and $p_c = 0.6$). For all algorithms, a budget of 5000 function evaluations has been given. It can be observed that the random search generator detects all nine sets, but the approximation of these sets is not sufficient (due to the lack of a local search procedure). $P_{Q,\epsilon}$-NSGA-II performs 'greedy', i.e., concentrates the search around $P_{0,0}$ and nearly neglects the other sets. The best approximation for this example is given by the result of $P_{Q,\epsilon}$-MOEA, which yields an approximation of all the nine sets.

Tables 1 and 2 show the values of the performance metrics proposed in Sec. III.B. Table 1 contains the performance metrics which use an expression of $P_{Q,\epsilon}$ (we have used a fine discretization in this case) and underline the impression obtained by Fig. 4. $P_{Q,\epsilon}$-NSGA-II yields (as its base algorithm NSGA-II) excellent values for the convergence toward the set of interest (i.e., dist(A_2, $P_{Q,\epsilon}$) and $GD_x(A_2)$), and since the image of the neighborhood of $P_{0,0}$ already forms $F(P_{Q,\epsilon})$, also excellent values for the convergence in image space. On the other side, since $P_{Q,\epsilon}$-NSGA-II does, due to its selection mechanism, not have an evolution pressure toward the regions around the locally optimal sets (32), the values which measure the spread along $P_{Q,\epsilon}$ (i.e., dist($P_{Q,\epsilon}$, A_2) and $IGD_x(A_2)$) cannot compete with the ones of $P_{Q,\epsilon}$-MOEA.

The results obtained by the set coverage metric in Table 2, however, are not that conclusive since only the performance in image space is considered which is not sufficient in this case. The only conclusion which can be drawn from these values is that the random search procedure is outperformed by both evolutionary strategies.

B. Two Impulse Transfer to Asteroid Apophis

For the biimpulse problem we analyze an apparently simple case: the direct transfer from the Earth to the asteroid Apophis. The contour lines of the sum of the two Δv's are represented in Fig. 5a for $t_0 \in [3675, 10{,}500]^T$ MJD2000

Table 1 Different performance metrics applied on the numerical results of the random search (A_1), $P_{Q,\epsilon}$-NSGA-II (A_2), and $P_{Q,\epsilon}$-MOEA (A_3) of MOP (30). The results are averaged over 30 independent test runs, the best solutions are in bold

Performance metrics	A_1	A_2	A_3
$d_H(A, P_{Q,\epsilon})$	5.281	7.653	**0.539**
dist($A, P_{Q,\epsilon}$)	0.262	**0.140**	0.157
dist($P_{Q,\epsilon}, A$)	5.281	7.653	**0.539**
$GD_x(A)$	0.026	**0.002**	**0.002**
$IGD_x(A)$	0.061	0.152	**0.004**
$d_H(F(A), F(P_{Q,\epsilon}))$	0.219	**0.081**	0.112
dist($F(A), F(P_{Q,\epsilon})$)	0.195	**0.081**	0.083
dist($F(P_{Q,\epsilon}), F(A)$)	0.291	**0.066**	0.112
$GD_y(A)$	0.011	0.001	**0**
$IGD_y(A)$	0.003	**0**	**0**

Table 2 Set coverage metric for the numerical results of the three algorithms (A_i as in Table 1), averaged over 30 test runs

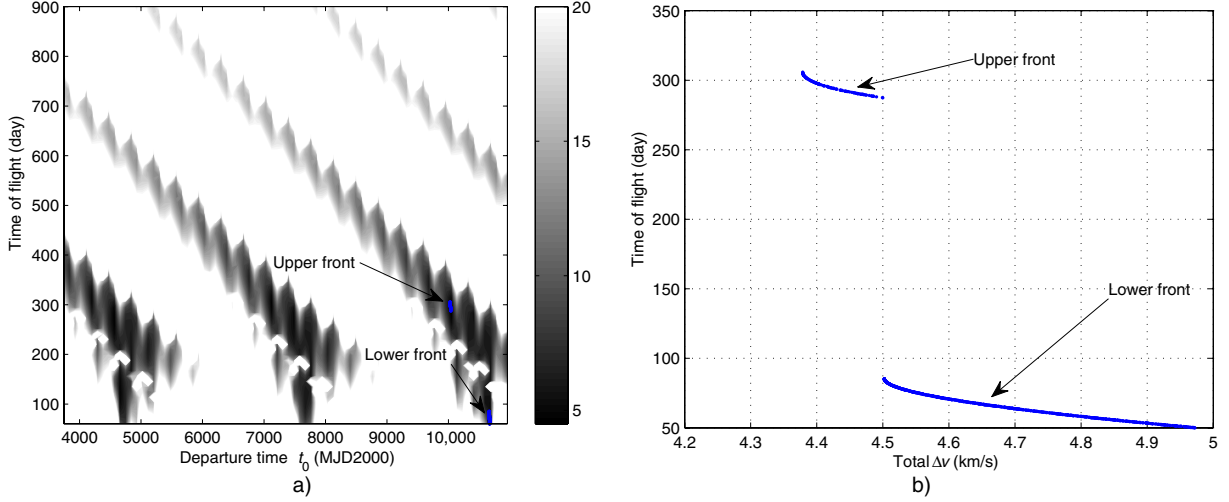|	$C_{-\epsilon}(A, B)$	$C_{-\epsilon}(B, A)$
$A = A_1, B = A_2$	0	0.407
$A = A_1, B = A_3$	0	0.412
$A = A_2, B = A_3$	0.045	0.001

Fig. 5 a) Earth–Apophis search space and b) Pareto front.

and $T \in [50, 900]$ days. The intervals for t_0 and T were chosen in such a way that a wide range of launch opportunities are included.

As can be seen in the specified solution space, there is a large number of local minima. Each minimum has a different value but some of them are nested, very close to each other with similar values. For each local minimum, there can be a different front of locally Pareto optimal solutions. The global Pareto front should contain the best transfer with minimum total Δv and the fastest transfer with minimum T.

The best known approximation of the global Pareto front is represented in Fig. 5b and was obtained with an extension to multi-objective optimization (MOO) problems of the algorithm described by Vasile and Locatelli [5,11]. It is a disjoint front corresponding to two basins of attraction of two minima as can be seen in Fig. 5a. The lower front is made of solutions with a very low transfer time. The upper front, instead, is made of solutions with a much longer transfer time but a total Δv similar to the one of the solutions belonging to the lower front.

Besides containing local minima with similar Δv, the two basins of attraction present similar values of the first objective function. Converging to the upper front is therefore quite a challenge since the lower front has a significantly lower value of the second objective function. It is only when the optimizer converges to a vicinity of the local minimum of the upper front that the latter becomes not dominated by the lower front. The upper front contains the global minimum with a total $\Delta v = 4.3786$ k/s whereas the lower front contains only a local minimum. It should be noted that, though the front in Fig. 5b is the global one, it represents only two launch opportunities. Furthermore, for each launch opportunity we would need to characterize the space around each Pareto optimal point.

Figure 6 shows a result for $P_{Q,\epsilon}$-MOEA and using $\epsilon = (5, 5)$. Since apparently the transfer of 50 days can be reached from any starting date, the biobjective problem shrinks in practice down to a mono-objective problem with optimal image value around $y_0 = (5, 50)$. A search within $N(y_0, \epsilon, A)$ revealed different possible starting times which fall into three clusters: the preimages of $N(y_0, \epsilon, A)$ are all located around the points $c_1 = (4700, 50)$, $c_2 = (7700, 50)$, and $c_3 = (10,700, 50)$. That is, the starting time t_0 differs by 3000 days for neighboring solutions, and by 6000 days in total.

Note that, compared to the accurate solution of the global Pareto front, the extended ϵ-pareto set offers, as required, not only more launch opportunities but also the whole neighboring solutions for each one of them.

As a comparison we have used the classical NSGA-II to attack the problem (see Fig. 7, note the different scale of these figures to Fig. 6). As anticipated, NSGA-II computes a good approximation of the (very narrow) Pareto set, but in fact generates points only around c_3, the maximal difference according to t_0 is given by 35 days.

C. Sequence Earth–Venus–Mercury

For the MLTGA problem, we first consider a relatively simple but significant case: the sequence EVMe.
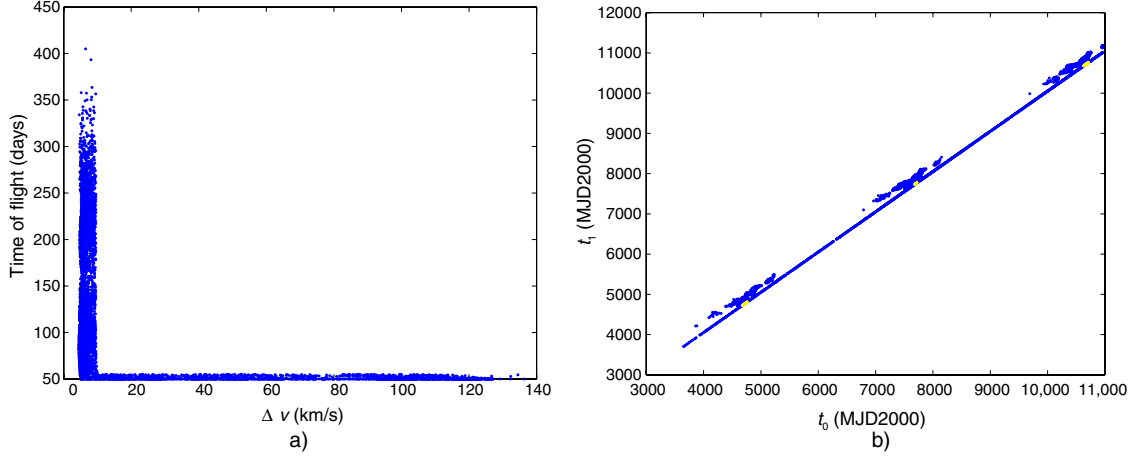
66

Fig. 6 Numerical result for Example 2 using $P_{Q,\epsilon}$-NSGA-II, in a) image space and b) parameter space.
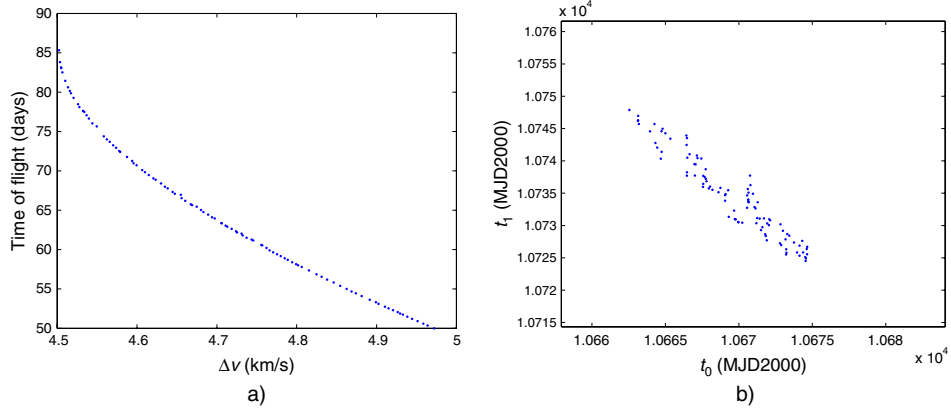

Fig. 7 Numerical result for Example 2 using NSGA-II, in a) Image space and b) parameter space.

For such a mission we have chosen to allow a deterioration of 5% of the mass fraction and of 20 days of the transfer time, compared to an optimal trajectory, which leads to $\epsilon = (0.05, 20)$. A solution vector for EVMe is given by

$$y = [t_0, t_1 - t_0, k_{2,1}, n_1, t_2 - t_1, k_{2,2}, n_2]^T \tag{33}$$

where

$$t \in T := [700, 1300] \times [800, 2100] \times [1300, 3600], \quad k_2 \in K_2 := [0, 1]^2 \tag{34}$$

and where the numbers of revolutions are fixed to $n_1 = 1$ and $n_2 = 7$, and choosing $r_{\min,1} = 6350$ and $r_{\min,2} = 1700$.

Figure 8 shows a numerical result of $P_{Q,\epsilon}$-MOEA, where we have taken an initial population consisting of 200 randomly chosen elements from the domain $Q = T \times K_2 \subset \mathbb{R}^5$, $p_c = 0.6$, $\Delta = \Delta^* = \epsilon/3$, and a budget of 50,000 function calls which took several minutes on an Intel Xeon 3.2 GHz processor.

Interesting for every nondominated point x_0 with $F(x_0) = y_0$ of an archive A is the set

$$N(y_0, \epsilon, A) := \{a \in A \ : \ F(a) \in B(y_0, \epsilon)\} \tag{35}$$

where $B(y, \epsilon) := \{x \in \mathbb{R}^k : |x_i - y_i| \leqslant \epsilon_i, i = 1, \ldots, k\}$, i.e., the set of solutions in A those images are close to y_0. Since in this design problem the starting date t_0 of the transfer is of particular interest one can, e.g., distinguish the entries in $N(y_0, \epsilon, A)$ by the value of t_0. For instance, the final archive displayed in Fig. 8a consists of 2305 solutions
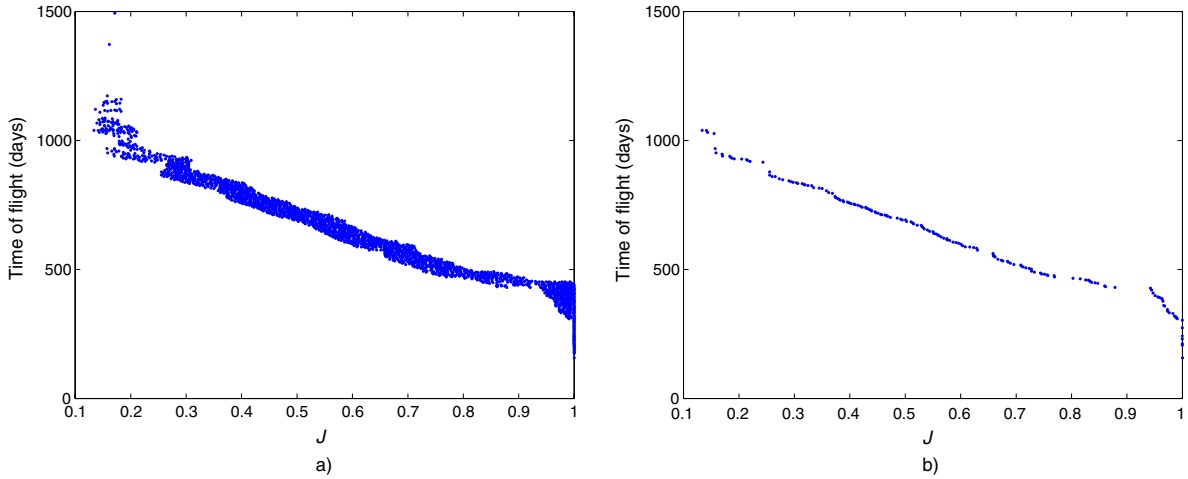
Fig. 8 Numerical result for sequence EVMe. At a) we show the final archive (i.e., the ϵ-efficient front) and at b) we show the set of non-dominated solutions which is, in this case, sufficient to display for the decision-making process.

whereof 344 are nondominated. The maximal difference of the value of t_0 for a point y_0 inside $N(y_0, \epsilon, A)$ is 461 days, and for 43 solutions this maximal difference is larger than one year (including also values Δt_0 of several days or months which can be also highly interesting for the decision-making process). Hence, the number of options for the DM is enlarged significantly in this example.

The consideration above leads to a natural way of presenting the large amount of data to the DM: it is sufficient to present the non-dominated front as in the classical multiobjective case. When the DM selects one solution y_0 the set $N(y_0, \epsilon, A)$ can be displayed, ordered by the value of t_0 (see Fig. 8b).

D. Sequence Earth–Venus–Earth–Jupiter

Finally, we consider the more complex sequence Earth–Venus–Earth–Jupiter (EVEJ) which involves seven free parameters (analog to (33)).

This design problem—as well as other problems of this kind—is characterized by a disconnected feasible domain, and the fraction of this set compared to the entire search space is tiny. To increase the performance of the search procedure, we followed [4] and have applied a space pruning algorithm on the search space leading to set $\mathcal{B}$ such
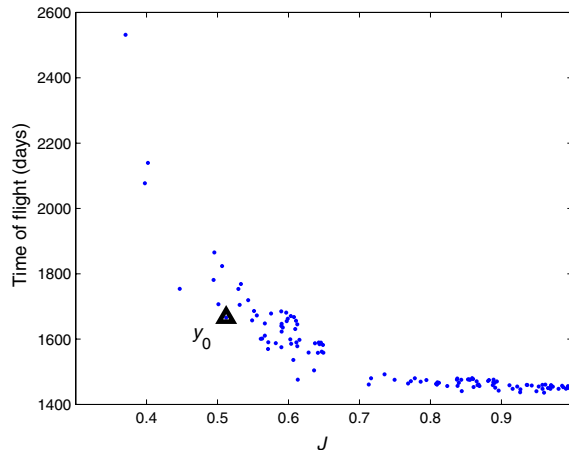

Fig. 9 Numerical result for sequence EVEJ using $P_{Q,\epsilon}$-NSGA-II.

68

that this set covers the feasible domain and where the volume of $\mathcal{B}$ is much less than the volume of the entire search space. Next, we have run $P_{Q,\epsilon}$-MOEA on these eight domains separately (population size 200, budget of 2000 function calls) and have merged the results afterward. We have chosen again $\epsilon = (0.05, 20)$, but $\Delta = (0, 0)$ since the feasible solutions are not too easy to find, and thus, every promising solution should be captured. Figure 9 shows one numerical result, which has been obtained within one hour of computational time.

As an example of the use of the result, we assume that the point y_0 has been selected by the DM (see Fig. 9). The set $N(y_0, \epsilon, A_{\text{final}})$ consists in this case of three solutions with starting times $t_{0,1} = 5085$, $t_{0,2} = 5562$, and $t_{0,3} = 6792$. Assuming that the values of y_0 have been chosen for the transfer and the archive A is the basis for the DM, then there are three possibilities: to launch the spacecraft in December 2013 (i.e., 5085 days after 01.01.2000), to launch it 16 months later, or to wait another 3.5 years after $t_{0,2}$. Similar statements hold in this example for all 15 non-dominated solutions x with $J = f_1(x) \geqslant 0.45$, and thus, also in this case the DM's decision space has been augmented by allowing approximate solutions.

V.   Conclusion and Future Work

In this paper, we have considered multiobjective space mission design problems with a novel prospective. For this kind of problems, it is desirable to identify not only the global Pareto set, but also a number of neighboring solutions as well as approximate solutions (which do not have to be in the neighborhood of an optimal solution). In particular, it was shown that each part of the Pareto set can belong to a different launch opportunity. To increase the reliability of the mission design, it is required to have a wide launch window for each launch opportunity (i.e., a large number of neighboring solutions with similar cost) and one or more backup launch opportunities (i.e., one or more nearly optimal sets).

To address this problem, we have proposed a new evolutionary strategy which aims for an approximation of $P_{Q,\epsilon}$, i.e., the solutions which are optimal up to a given (small) value of ϵ. As an example of its effectiveness, we have considered three design problems. The results indicate that the novel approach accomplishes its task within reasonable time and that the idea to include approximate solutions is indeed beneficial since in all cases the decision maker was offered with an enlarged set of useful solutions.

Though the algorithm proposed in this paper seems to be well-suited for the design problems under consideration, the authors think that its performance can be increased in general, and that further research on performance indicators, not using a given reference set, needs to be done.

Acknowledgments

References

[1] Coverstone-Caroll, V., Hartmann, J. W., and Mason, W. M., "Optimal Multi-Objective Low-Thrust Spacecraft Trajectories," *Computer Methods in Applied Mechanics and Engineering*, Vol. 39, 2000, pp. 387–402.

[2] Schütze, O., Coello Coello, C. A., Tantar, E., and Talbi, El-G., Computing Finite Size Representations of the Set of Approximate Solutions of An mop with Stochastic Search Algorithms," *GECCO'08: Proceedings of the 10th Annual Conference on Genetic and Evolutionary Computation*, ACM, New York, NY, 2008, pp. 713–720.

[3] Schütze, O., Vasile, M., Junge, O., Dellnitz, M., and Izzo, D., "Designing Optimal Low-Thrust Gravity-Assist Trajectories Using Space Pruning and A Multi-Objective Approach," *Engineering Optimization*, Vol. 41, No. 2, 2009, pp. 155–181.

[4] Vasile, M., Schütze, O., Junge, O., Radice, G., and Dellnitz, M., "Spiral Trajectories in Global Optimisation of Interplanetary and Orbital Transfers," Ariadna Study Rept. ao4919 05/4106, Contract No. 19699/nl/he, European Space Agency, 2006.

[5] Vasile, M., "Hybrid Behavioural-Based Multiobjective Space Trajectory Optimization," In *Multi-Objective Memetic Algorithms*, edited by C.-K. Goh, Y.S. Ong, and K. C. Tan, Studies in Computational Intelligence 171, Springer, Berlin, 2009, pp. 231–253.

[6] Coello Coello, C. A., Lamont, G. B., and Van Veldhuizen, D. A., *Evolutionary Algorithms for Solving Multi-Objective Problems*, 2nd ed., Springer, New York, NY, Sept. 2007.

[7] Laumanns, M., Thiele, L., Deb, K., and Zitzler, E., "Combining Convergence and Diversity in Evolutionary Multiobjective Optimization," *Evolutionary Computation*, Vol. 10, No. 3, 2002, pp. 263–282.

[8] Loridan, P., "ϵ-solutions in Vector Minimization Problems," *Journal of Optimization, Theory and Application*, Vol. 42, 1984, pp. 265–276.

[9] White, D. J., "Epsilon efficiency," *Journal of Optimization Theory and Applications*, Vol. 49, No. 2, 1986, pp. 319–337.

[10] Schütze, O., Coello Coello, C. A., and Talbi, El-G., "Approximating the ϵ-Efficient Set of An MOP with Stochastic Search Algorithms," *Mexican International Conference on Artificial Intelligence* (*MICAI-2007*), edited by A. Gelbukh and A. F. Kuri Morales, Springer, Berlin, 2007, pp. 128–138.

[11] Vasile, M., and Locatelli, M., "A Hybrid Multiagent Approach for Global Trajectory Optimization," *Journal of Global Optimization*, Vol. 44, No. 4, 2009, pp. 461–479.

[12] Schütze, O., Vasile, M., and Coello Coello, C. A., "Approximate Solutions in Space Mission Design Pallel Problem Solving from Nature – PPSN X", *Lecture Notes in Computer Science*, Vol. 5199, No. 2008, 2008, pp. 805–814.

[13] Deb, K., Mohan, M., and Mishra, S., "Evaluating the ϵ-Dominated Based Multi-Objective Evolutionary Algorithm for a Quick Computation of Pareto-Optimal Solutions," *Evolutionary Computation*, Vol. 13, No. 4, 2005, pp. 501–525.

[14] Hanne, T., "On the Convergence of Multiobjective Evolutionary Algorithms," *European Journal of Operational Research*, Vol. 117, No. 3, 1999, pp. 553–564.

[15] Rudolph, G., and Agapie, A., "Convergence Properties of Some Multi-Objective Evolutionary Algorithms," *CEC 2008: Proceedings of the 2000 Conference on Evolutionary Computation*, edited by A. Zalzala *et al.*, IEEE Press, Piscataway, NJ, Vol. 2, 2000, pp. 1010–1016.

[16] Knowles, J., and Corne, D., "Bounded Pareto Archiving: Theory and Practice," *Metaheuristics for Multiobjective Optimisation*, edited by X. Gandibleux, M. Sevaux, K. Sörensen, and V. T'kindt, Lecture Notes in Economics and Mathematical Systems 535, Springer, Berlin, 2004, pp. 39–64.

[17] Deb, K., Pratap, A., Agarwal, S., and Meyarivan, T., "A Fast and Elitist Multiobjective Genetic Algorithm: NSGA–II," *IEEE Transactions on Evolutionary Computation*, Vol. 6, No. 2, 2002, pp. 182–197.

[18] Pareto, V., *Manual of Political Economy*, Macmillan, New York, NY, 1971 (original edition in French in 1927).

[19] Deb, K., and Goldberg, D. E., "An Investigation of Niche and Species Formation in Genetic Function Optimization," *Proceedings of the Third International Conference on Genetic Algorithms*, edited by J. David Schaffer, Morgan Kaufmann, San Mateo, CA, 1989, pp. 42–50.

[20] Goldberg, D. E., and Richardson, J., "Genetic Algorithm with Sharing for Multimodal function Optimization," *Genetic Algorithms and Their Applications: Proceedings of the Second International Conference on Genetic Algorithms*, edited by John J. Grefenstette, Lawrence Erlbaum, New Jersey, NJ, 1987, pp. 41–49.

[21] Battin, R. H., *An Introduction to the Mathematics and Methods of Astrodynamics*, AIAA, Reston, VA, 1999.

[22] Petropoulos Longuski, A. E., James, M., and Vinh, N. X., "Shape-Based Analytic Representations of Low-Thrust Trajectories for Gravity-Assist Applications", *Proceedings of the AAS/AIAA Astrodynamics Conference*, Girdwood, AK, 16–19 Aug. 1999.

[23] Izzo, D., "Lambert's Problem for Exponential Sinusoids," TRACT/ESTEC Internal Rept., April 2005.

[24] Deb, K., and Agrawal, R. B., "Simulated Binary Crossover for Continuous Search Space," *Complex Systems*, Vol. 9, 1995, pp. 115–148.

[25] Van Veldhuizen, D. A., "Multiobjective Evolutionary Algorithms: Classifications, Analyses, and New Innovations," PhD Thesis, Dept. Electrical and Computer Engineering, Graduate School of Engineering, Air Force Institute of Technology, Wright-Patterson AFB, Ohio, May 1999.

[26] Zitzler, E., "Evolutionary Algorithms for Multiobjective Optimization: Methods and Applications," PhD Thesis, ETH Zurich, Switzerland, 1999.

[27] Rudolph, G., Naujoks, B., and Preuss, M., "Capabilities of EMOA to Detect and Preserve Equivalent Pareto Subsets," *EMO 2007: Proceedings of the 4th International Conference on Evolutionary Multi-Criterion Optimization*, edited by S. Obayashi, K. Deb, C. Poloni, T. Hiroyasu, and T. Murata, Lecture Notes in Computer Science 4403, Springer, Berlin, 2007, pp. 36–57.

Roy Sterritt
Associate Editor